Available online at www.sciencedirect.com
ScienceDirect
Surface & Coatings Technology 202 (2008) 3772–3776
SURFACE & COATINGS TECHNOLOGY
www.elsevier.com/locate/surfcoat

The effect of current density on the grain size of electrodeposited nanocrystalline nickel coatings

A.M. Rashidi [a,b,*], A. Amadeh [a]

[a] School of Metallurgy & Materials Engineering, Faculty of Engineering, University of Tehran, P.O. Box 11155-4563, Tehran, Iran
[b] Faculty of Engineering, Razi University, P.O. Box 67149-67346, Kermanshah, Iran

Received 28 October 2007; accepted in revised form 17 January 2008
Available online 26 January 2008

Abstract

The aim of this work was to investigate the effect of current density on the grain size of electrodeposited nickel coatings. For this purpose, nanocrystalline nickel coatings were deposited from a Watts bath containing 5 g/l sodium saccharin as an additive, by direct current electroplating at different current densities. X-ray diffraction analysis and modified Williamson–Hall relation were used to determine the average grains size of the coatings. The experimental results showed that the coating grains size decreased sharply by increasing the current density from 10 mA/cm^2 to 75 mA/cm^2. Nanocrystalline nickel coating with average grain size smaller than 30 nm can be achieved at the current densities higher than 50 mA/cm^2. Furthermore, a general and simple theoretical model based on atomistic theory of electrocrystallization has been made in order to find out the relationship between the grain size and current density. According to this model the variation of log (d) versus log (i) was linear which is in accordance with experimental results for the current densities lower than 75 mA/cm^2.

Keywords: Current density; Grain size; Nanocrystalline; Nickel coating; Theoretical model

1. Introduction

Recently, the production and characterization of nanocrystalline coatings, with the grain size typically smaller than 100 nm, have been the subject of intensive researches [1,2]. Various techniques, such as electrodeposition, physical vapor deposition (PVD), chemical vapor deposition (CVD), laser beam deposition, ion implantation, plasma and high-velocity oxygen fuel (HVOF) spraying have been developed for synthesis of these coatings [2,3]. Among these methods, electrodeposition has been recognized as the most technologically feasible and economically superior technique for production of nanocrystalline coatings with low residual porosity. Compared to other methods, the advantages of electrodeposition are: (a) low cost and industrial applicability, as it involves little modification of existing electroplating technologies, (b) easy of control, as the electrodeposition parameters can be easily tailored to meet the required crystal size, microstructure and chemistry of products, (c) versatility, as the process can produce a wide variety of pore free coatings and (d) high production rates [4,5].

It has long been known that the properties of electrodeposits are dependent on their microstructure, which can be substantially influenced by the deposition parameters [6–11]. The tailoring of the properties of nanocrystalline coatings through synthesis process control requires a profound understanding of the process–microstructure relations of the involved materials. It is of great interest to understand the relation between the grain size of nanocrystalline coatings and their synthesis technique parameters both from the fundamental and performance standpoints because the properties of these coatings is intrinsically size dependent. For example, a decrease in the grain size from 100 μm to 10 nm, increases the hardness of electrodeposited nickel coating from ~1.5 GPa to ~6.5 GPa [12]. Further grain refinement appears to decrease the hardness

* Corresponding author. School of Metallurgy & Materials Engineering, Faculty of Engineering, University of Tehran, P.O. Box 11155-4563, Tehran, Iran. Tel.: +98 831 4274535; fax: +98 831 4274542.
E-mail addresses: rashidi1347@razi.ac.ir (A.M. Rashidi), amadeh@ut.ac.ir (A. Amadeh).

0257-8972/$ - see front matter © 2008 Elsevier B.V. All rights reserved.
doi:10.1016/j.surfcoat.2008.01.018

of the coating [13]. This behavior has also been observed in other nanocrystalline coatings [14,15].

The current density plays an important role on the grain size of electrodeposited coatings. In general, high current densities promote the grain refinement [6–10]. An increase in the current density results in a higher overpotential that increases the nucleation rate [16]. Moreover, when the current density increases, the cluster density can be increased [17]. However, between the numerous studies which have investigated this effect for nanocrystalline nickel coatings [11,18–23], some has reported a contrary behavior [11,18,19,23]. Hence, the effect of current density on the average grain size of electrodeposited nanocrystalline nickel coating still needs more experimental and theoretical studies.

The purpose of this investigation was to study the influence of current density on the average grain size of electrodeposited nanocrystalline nickel coating. Based on the atomistic theory of nucleation, a general quantitative relationship was obtained between the average grain size and current density. Theoretical findings were then discussed in connection with experimental results.

2. Experimental procedure

Nanocrystalline nickel coatings were deposited on copper substrates by direct current (DC) electroplating using a circulated electrolyte system described by Tóth-Kádár et al. [23]. A nickel sheet of 99.99% purity with dimensions of $100\times50\times5$ mm^3 was used as anode and pure annealed copper plate with dimensions of $20\times15\times2$ mm^3 as cathode materials.

Prior to deposition, the copper substrates were mechanically polished with silicon carbide papers of 400, 600, 800, 1200 grits and alumina suspensions of 8, 1 and 0.25 μm, then rinsed with distilled water and activated in 10% H_2SO_4 solution at room temperature for 30 s. Nickel coatings were deposited from a Watts bath containing 300 g/l nickel sulfate ($NiSO_4{\cdot}6H_2O$), 30 g/l nickel chloride ($NiCl_2{\cdot}6H_2O$), 30 g/l boric acid (H_3BO_3) and 5 g/l sodium saccharin ($C_7H_4NO_3S.Na$) as a grain refiner and stress reliever agent. The current density varied in the range of 10–300 mA/cm^2. The plating temperature was kept at 55 °C and pH of the bath was adjusted to 4.0 ± 0.2 by addition of drops of HCl (1 N) or NaOH (1 N). The coatings thickness was fixed to about 100 μm by controlling the plating time.

X-ray diffraction (XRD) studies were carried out using a Philips X'Pert-Pro instrument operated at 40 kV and 30 mA with CoKα radiation ($\lambda=1.789$ A°) at a scan rate of 0.05° s^{-1} in the range of 40–130° and 0.02° step size. The average grain size of the nickel coatings was calculated from XRD patterns via modified Williamson–Hall relation given by [24,25]:

$$\Delta K_{\mathrm{FWHM}} = \frac{0.9}{d} + \left(K\overline{C}^{1/2}\right)^2 + O\left(K\overline{C}^{1/2}\right)^4 \quad (1)$$

where $\Delta K_{\mathrm{FWHM}} = \frac{2\beta\cos(\theta_0)}{\lambda}, K = \frac{2\sin(\theta_0)}{\lambda}$, λ and θ_0 are the wavelength of radiation and the Bragg diffraction angle, respectively, α is a numerical constant depending on the dislocation density, O stands for higher order terms in $K^2\overline{C}$,$\overline{C}$ is the average dislocation contrast factor calculated according to Ref. [26] and β is the intrinsic (true) profile full width at half maximum intensity (FWHM). The β parameter was calculated using the Cauchy–Cauchy relation [2]:

$$\beta = \beta_{\mathrm{exp}} - \beta_{\mathrm{ins}} \quad (2)$$

where β_{exp} and β_{ins} are the FWHM of experimental and instrumental profiles, respectively. β_{exp} and β_{ins} were determined by Lorentzian (Cauchy) curve fitting using a custom-built Matlab software. The annealed nickel with average grain size of 30 μm was used as reference sample. The average grain size of the coatings was calculated by a plot of ΔK_{FWHM} versus $\left(K\overline{C}^{1/2}\right)^2$, using the (111), (200), (220), (311) and (222) diffraction peaks and curve fitted by applying a second-order polynomial.

3. Results and discussion

3.1. Experimental results

Fig. 1 shows the XRD patterns of the nickel coatings produced at various current densities. For comparison, the XRD pattern of reference sample (annealed nickel) has also been shown in this figure. It can be observed that the crystal structure of the coatings is pure fcc nickel and no characteristic peaks of other phases have been recorded.

In Fig. 1, the peak broadening of the samples is not completely clear, because the FWHM is small. In order to have a better distinction between the samples, it is necessary that the intensity of (hkl) reflection, (I_{hkl}), be normalized in the form of $I_{N,\mathrm{hkl}}=I_{\mathrm{hkl}}/I_{p,\mathrm{hkl}}$ and $I_{N,\mathrm{hkl}}$ be plotted versus diffraction angle, (2θ) for the same reflection. For this purpose, the intensity of (111) reflection for nickel coatings deposited at various current densities and also reference sample (annealed nickel) were normalized and presented in Fig. 2.

As it can be seen, the XRD peaks of nickel coatings are wider than the annealed nickel and the peak width increases by increasing the current density. The variation of the average grain size, calculated from modified Williamson–Hall relation, versus current density has been presented in Fig. 3. For comparison, the data reported by some other researchers for nickel deposits from Watts bath [21,27–31] and nickel sulfate electrolyte [1] were also presented in this figure. As seen, the results are in

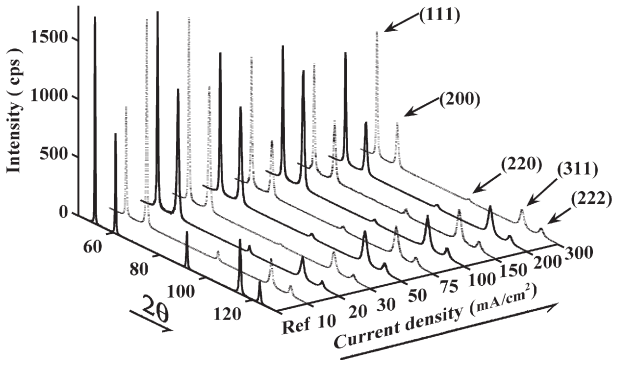

Fig. 1. XRD patterns of Ni coatings produced at various current densities.

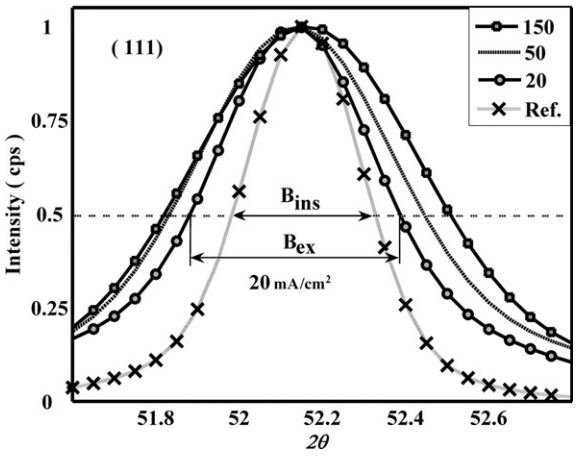

Fig. 2. The normalized (111) reflection peaks of nickel coatings at the current densities of 20, 50 and 150 mA/cm^2 and annealed nickel (Ref. sample).

reasonable agreement and the scattering of the data for a given current density comes mainly from the fact that the deposition conditions and also, the methods used for determination of grain size were not quite the same.

It is evident from Fig. 3 that the grain size of the coatings decreases rapidly by increasing the current density before leveling off at the current densities higher than 75 mA/cm^2. The grain size decreases from 182 nm to about 24 nm, when the current density increases from 10 mA/cm^2 to 75 mA/cm^2. Further increase in current density from 75 mA/cm^2 to 300 mA/cm^2 has no significant effect on the grain size of the coating. This behavior is consistent with the works conducted by Pin-Qiang et al. [21] and Wang et al. [1].

According to general patterns presented by Winand [6–8] and Dini [9] it is expected that the grain size of the deposits decreases by increasing the current density. The experimental results indicated in Fig. 3 are consistent with this general relationship up to the current density of 75 mA/cm^2, but there is a deviation beyond this point. The increase in the crystallite size associated by increasing the current density has also been reported in DC electrodepositions of nickel from other bath types [11,18,32–35]. Their results are quite opposite with general relationship. Cziráki et al. [34] attributed the increase in the grain size at relatively high current densities to a decrease in the concentration of Ni ions at the deposit–electrolyte interface. Ebrahimi et al. [18] suggested that this phenomenon can be attributed to the co-deposition of hydrogen at the cathode interface. The changes in the surface energy and growth mechanisms in the presence of hydrogen are responsible for the increase in the crystallite size by increasing of current density [18]. Moreover, based on electrocrystallization consideration, it is possible to indicate the deviation from general relationship could be attributed to the difference of kinetic parameters in different baths.

3.2. Theoretical considerations

Electrodeposition is a complex and usually multi-step electrochemical process. The analysis of the effect of current density on the grain size of the deposits will become complicate by considering real systems, and is beyond the scope of this paper. For simplicity, it is assumed that (i) the charge transfer is a slow process, (ii) all the steps that precede or follow the chemical and electrochemical reactions are negligible and (iii) the clusters grow in a hemispherical shape.

The size of a cluster with radius $R(t)$ is a function of time, overpotential, exchange current density, etc. Some relationships and detailed informations can be found in Refs.[36,37]. A simple relationship between the size of the cluster [$d(t)=2R(t)$] and the above parameters can be expressed as [36]:

$$d(t) = \frac{2V_M}{zF}\left(i_\circ f(\eta)\right)t \tag{4}$$

where i_o (A/cm^2) is the exchange current density, V_M (cm^3/mol) is the molar volume of the deposit, z is the valence number of reduced ion, F(As/mol) is the Faraday's constant, t (s) is the time of cluster growth and $f(\eta)$ is the function of overpotential according to:

$$f(\eta) = \exp\left(\frac{\alpha zF\eta}{RT}\right) - \exp\left(\frac{(1-\alpha)zF\eta}{RT}\right) \tag{5}$$

where α is the cathodic charge transfer coefficient, η is the overpotential, R is the molar gas constant and T is the absolute temperature.

Using the average time of cluster growth ($\bar{t}_g$), the average grain size ($\bar{d}$) can be obtained from Eq. 4. The dependence of the average time of cluster growth to the overpotential can be achieved from the theoretical potentiostatic current-time transient model. The current transient is characteristic of nucleation and phase growth of the deposits [38]. According to the theoretical models of current transient [36,39] due to the growth of either independent nuclei alone or simultaneous nucleation, the current increases up to a maximum value at the time $t=t_m$, where the growth centers begin to overlap. The result of this overlap is the development of local concentration and the growing nuclei cannot grow freely in all directions, since they will impinge on each other [40,41]. The growth will stop at the point of contact, resulting in the limitation of the size of growth

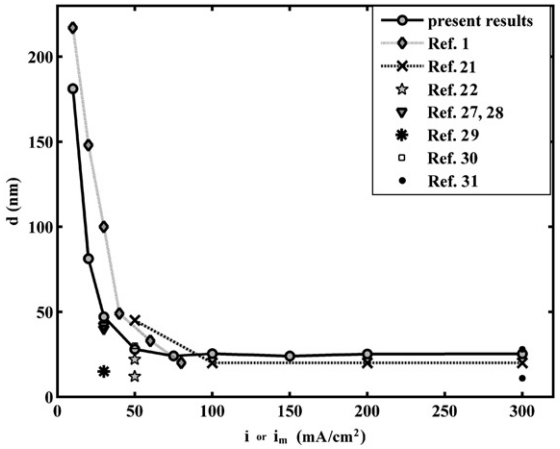

Fig. 3. Variation of the grain size of Ni deposits as a function of current density.

center [41]. The t_m is a function of overpotential. The relationship between t_m and η can be found in the Ref. [36]. Since t_m and t_g refer to the time of cluster growth with different duration, it could be suggested that their dependence on η is analogous :

$$\bar{t_g} = B_1 I_{st}^{-1/3} \left(i_\circ f(\eta) \right)^{-2/3} \quad (6)$$

where B_1 is constant and I_{st} is stationary nucleation rate.

Using the equation of Butler–Volmer (Erdey–Grúz–Volmer) [42–45], Eq. 5 reduces to $i_\circ f(\eta)$=i. Substituting Eq. 6 in Eq. 4 and using $i_\circ f(\eta)=i$ one obtains:

$$\bar{d} = \frac{2B_1 V_M}{zF} \left(\frac{i}{I_{st}} \right)^{1/3} \quad (7)$$

Based on the classical and the atomistic theory, the theoretical models have been derived for the stationary nucleation rate [36,46–54]. The classical model can be used to predict the size of sufficiently large critical clusters, while the atomistic model is valid when the critical cluster is very small [36]. Experiments have shown that in most of the cases of metal deposition, the size of the critical clusters is of atomic dimensions [46]. Thus, it is necessary to consider the atomistic theory of electrocrystallization [36,50–54]. According to this theory, the stationary nucleation rate can be expressed as:

$$I_{st} = A_0 \mathrm{Exp}(A_1 \eta) \quad (8)$$

where A_0 is constants and A_1 is nucleation rate slope, i.e., the slope of ln $(I_{st})-\eta$ curve.

On the other hand, when the overpotential becomes more negative, usually greater than −100 mV, the Erdey–Grúz–Volmer equation can be reduces to Tafel equation and rewritten as [41]:

$$\eta = \frac{\beta}{2.3} . \ln \left(\frac{i}{i_0} \right) \quad (9)$$

where β is the Tafel slope. Introducing Eq. 9 into Eq. 8, it can be obtained:

$$I_{st} = A_0 \left(\frac{i}{i_0} \right)^n \quad (10)$$

in which $n = \frac{\beta \cdot A_1}{2.3}$ is constant. Thus, Eq. 7 can be rewritten as:

$$\bar{d} = \frac{2B_1 V_M i_0^{n/3}}{zF A_0^{1/3}} \times_i (1-n)/3 \quad (11)$$

Thus the current density dependence of average grain size can be expressed as a linear relationship:

$$\log\left(\bar{d}\right) = B_m + \frac{1-n}{3} \log(i) \quad (12)$$

where $B_m = \log\left(\frac{2B_1 V_M i_0^{n/3}}{zF A_0^{1/3}} \right)$ is a constant.

According to Eq. 12, by increasing the current density, the grain size decreases if $n>1$ and increases when $n<1$. On the other hand, n is the function of Tafel slope and nucleation rate slope. Hence, Eq. 12 shows that the effect of current density on the grain size depends on the polarization and nucleation parameters such as Tafel slope and nucleation rate slope. In the case of electrodeposition of nickel, the values reported for nucleation rate slope [40,55–58] and also the Tafel slope [40,58–61] indicated that these parameters and as a results, the value of n varies with bath composition. Therefore, based on Eq. 12, an increase in current density can lead to different effect on the grain size of nickel deposited from different baths.

Moreover, Eq. 12 predicts that the plot of log (d) versus log (i) should follow a linear relationship. It is therefore possible to test the model by plotting the experimental data in the logarithmic forms. For this purpose, the logarithmic plot of experimental data (Fig. 3) has been represented in Fig. 4. As seen, for current density up to 75 mA/cm^2, the experimental curves have the same shape as predicted by Eq. 12 for $n>1$. Nevertheless, more experimental work is required for evaluation of this model.

In Fig. 4, for current densities higher than 75 mA/cm^2 a clear deviation of experimental data from theoretical linear form is observed. This phenomenon can be attributed to:

- The assumptions made in the derivation of the model at high current densities could be invalid. At high current densities, the rate of cluster growth is controlled by mass transfer and also the occurrence of other electrochemical reactions such as evolution of hydrogen at cathode surface.
- The passivation of cathode surface by precipitation of a nickel hydroxide which dominates the nucleation process [62]. In this case, any current density increase would result in an increase in the passivated area, instead of increase in nucleation rate.
- The change in Tafel slope at high current densities. The current density-potential curves presented by [59,63] show two distinct Tafel slopes such that at high current densities, the value of Tafel slope is less than low current densities.
- The co-deposition of hydrogen at cathode surface. This phenomenon can lead to the change in the surface energy and

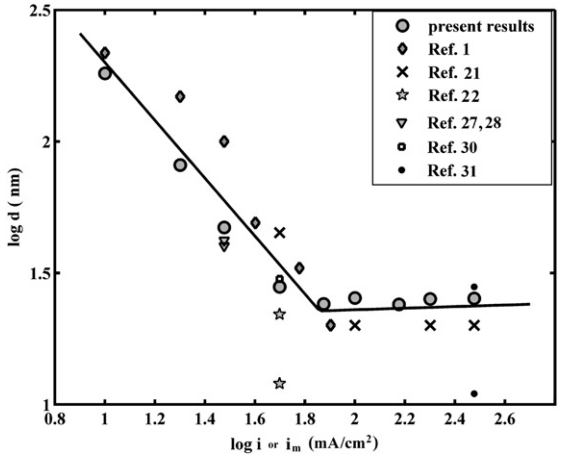

Fig. 4. Dependence of the grain size of Ni deposits on the current density, according to Eq. 12.

the growth mechanism [18] and also the distribution of applied currents between the reduction of Ni^{2+} and H^{+} ions. In the latter case, despite an increase in applied current density, the pure current density available for nickel deposition does not increase considerably.

4. Conclusions

Analysis of the theoretical and experimental results led to the following conclusions:

1. Nanocrystalline nickel coatings with average grains size smaller than 30 nm can be applied from Watts bath containing 5 g/l sodium saccharin at the current densities higher than 50 mA/cm^2.
2. An increase in current density up to 75 mA/cm^2 resulted in a decrease in the average grain size of nickel coatings.
3. Theoretical model predicted the linear relationship between log (d) and log (i) which is in accordance with experimental results for the current densities lower than 75 mA/cm^2.

Acknowledgement

This research was supported by the University of Tehran and Razi University. The Authors would like to thank them for the financial support of this work.

References

[1] L. Wang, Y. Gao, T. Xu, Q. Xue, Mater. Chem. Phys. 99 (2006) 96.
[2] S.C. Tjong, H. Chen, Mater. Sci. Eng. R 45 (2004) 1.
[3] C. Suryanarayana, C.C. Koch, Hyperfine Interactions 130 (2000) 5.
[4] U. Erb, Canadian Metall. Quar. 34 (1995) 272.
[5] A.M. El-Sherik, U. Erb, J. Mater. Sci. 30 (1995) 5743.
[6] R. Winand, Hydrometallurgy 29 (1992) 567.
[7] R. Winand, Electrochim. Acta 39 (1994) 1091.
[8] R. Winand, J. Appl. Electrochem. 21 (1991) 377.
[9] J.W. Dini, Electrodeposition: The Material Science of Coatings and Substrates, Noyes Publications, 1993.
[10] J.W. Dini, Plat. Surf. Finish. 75 (1988) 11.
[11] I. Bakony, E. Tóth-Kádár, L. pogány, Á. Cziráki, I. Gerőcs, K. Varga-Josepovits, B. Arnold, K. Wetig, Surf. Coat. Tech. 78 (1996) 124.
[12] A.M. El-Sherik, U. Erb, G. Palumbo, K.T. Aust, Scr. Metall. Mater. 27 (1992) 1185.
[13] C.A. Schuh, T.G. Nieh, T. Yamasaki, Scr. Mater. 46 (2002) 735.
[14] D.A. Konstantinidis, E.C. Aifantis, Nanostr. Mater. 10 (1998) 1111.
[15] S. Takeuchi, Scr. Mater. 44 (2001) 1483.
[16] W. Schmickler, Interfacial Electrochemistry, OUP, Oxford, 1996.
[17] R. Winand, Electrochim. Acta, 43 (1998) 2925.
[18] F. Ebrahimi, Z. Ahmed, J. Appl. Electrochem. 33 (2003) 733.
[19] N.S. Qu, D. Zhu, K.C. Chan, W.N. Lei, Surf. Coat. Tech. 168 (2003) 123.
[20] A.M. El-Sherik, U. Erb, J. Page, Surf. Coat. Tech. 88 (1996) 70.
[21] D. Pin-Qiang, Y. Hui, L. Qiang, Trans. Mater. Heat Treatment 25 (2004) 1283.
[22] R.T.C. Choo, J.M. Togri, A.M. El-Sherik, U. Erb, J. Appl. Electrochem. 25 (1995) 384.
[23] E. Tóth-Kádár, I. Bakonyi, A. Sólyom, J. Hering, G. Konczos, F. Pavlyák, Surf. Coat. Tech. 31 (1987) 31.
[24] T. Ungár, J. Gubicza, G. Ribárik, A. Borbély, J. Appl. Crys. 34 (2001) 298.
[25] P. Scardi, M. Leoni, R. Delhez, J. Appl. Crys. 37 (2004) 381.
[26] T. Ungár, I. Dragomir, Á. Révész, A. Borbély, J. Appl. Crys. 32 (1999) 992.
[27] X. Peng, Y. Zhang, J. Zhao, F. Wang, Electrochim. Acta 51 (2006) 4922.
[28] C. Gu, J. Lian, J. He, Z. Jiang, Q. Jiang, Surf. Coat. Tech. 200 (2006) 5413.
[29] D.J. Guidry, M.Sc. Thesis, Louisiana State University, May 2002.
[30] K.S. Kumar, S. Suresh, M.F. Chisholm, J.A. Horton, P. Wang, Acta Mater. 51 (2003) 387.
[31] R. Mishra, B. Basu, R. Balasubramaniam, Mater. Sci. Eng. A 373 (2004) 370.
[32] K.L. Morgan, Z. Ahmed, F. Ebrahimi, Mat. Res. Soc. Symp. 634 (2001) Materials Research Society.
[33] A.A. Rasmussen, P. Møller, M.A.J. Somers, Surf. Coat. Tech. 200 (2006) 6037.
[34] Á. Cziráki, B. Fogarassy, I. Gerőcs, E. Tóth-Kádár, I. Bakony, J. Mater. Sci. 29 (1994) 4771.
[35] I. Bakony, E. Tóth-Kádár, T. Tarnóczi, L.K. Varga, Á. Cziráki, I. Gerőcs, B. Fogarassy, Nonstr. Mater. 3 (1993) 155.
[36] A. Milchev, Electrocrystallization, Fundamentals of Nucleation and Growth, Kluwer Academic Publishers, 2002.
[37] A. Milchev, J. Electroanal. Chem. 612 (2008) 42.
[38] A. Saraby-Reintjes, M. Fleischmann, Electrochim. Acta 29 (1984) 557.
[39] B. Scharifker, G. Hills, Electrochim. Acta 28 (1983) 879.
[40] M.Y. Abyaneh, M. Fleischmann, J. Electroanal. Chem. 119 (1981) 187.
[41] M. Paunovic, M. Schlesinger, Fundamentals of Electrochemical Deposition, Wiley Interscience Publication, John Wiley & Sons, Inc., 1998.
[42] J.A.V. Butler, Trans. Farad. Soc. 19 (1924) 734.
[43] J.A.V. Butler, Trans. Farad. Soc. 28 (1932) 379.
[44] T. Erdey-Gruz, M. Volmer, Z. Phys. Chem. A 150 (1930) 203.
[45] T. Erdey-Gruz, M. Volmer, Z. Phys. Chem. A 157 (1931) 165.
[46] E. Budevski, G. Staikovb, W.J. Lorenz, Electrochim. Acta 45 (2000) 2559.
[47] J. Mostany, J. Mozota, B.R. Scharifker, J. Electroanal. Chem. 177 (1984) 25.
[48] A. Serruya, J. Mostany, B.R. Scharifker, J. Electroanal. Chem. 464 (1999) 39.
[49] M. Fleischmann, H.R. Thirsk, Trans. Faraday Sot. 51 (1955) 71.
[50] G. Staikov, A. Milchev, Electrocrystallization in Nanotechnology, Wiley-VCH Verlag GmbH & Co. KGaA, Weinheim, 2007.
[51] A. Milchev, L. Heerman, Electrochim. Acta 48 (2003) 2903.
[52] A. Milchev, S. Stoyanov, R. Kaischew, Thin Solid Films 22 (1974) 255.
[53] A. Milchev, S. Stoyanov, R. Kaischew, Thin Solid Films 22 (1974) 267.
[54] A. Milchev, Contemp. Phys. 32 (1991) 321.
[55] A.G. Munoz, D.R. Salinas, J.B. Bessone, Thin Solid Films. 429 (2003) 119.
[56] M.Y. Abyaneh, M. Fleischmann, J. Electroanal. Chem. 530 (2002) 89.
[57] A.N. Correia, S.A.S. Machado, L.A. Avaca, J. Electroanal. Chem. 488 (2000) 110.
[58] Ž. Petrovića, M. Metikoš-Huković, Z. Grubač, S. Omanović, Thin Solid Films 513 (2006) 193.
[59] O. Aaboubi, J. Amblard, J.P. Chopart, A. Olivier, J. Phys. Chem. B, 105 (2001) 7205.
[60] U.S. Mohanty, B.C. Tripathy, P. Singh, S.C. Das, Miner. Eng. 15 (2002) 531.
[61] M.A.M. Ibrahim, J. Appl. Electrochem. 36 (2006) 295.
[62] P.V. Brande, A. Dumont, R. Winand, J. Appl. Electrochem. 24 (1994) 201.
[63] I. Epelboin, R. Wiart, J. Electrochem. Soc. 118 (1971) 1578.